Synthesis, magnetic and electromagnetic wave absorption properties of planar anisotrop Y_2Co_{17}@SiO_2 rare earth soft magnetic composites

Liang Qiao(乔亮)[1,†], Cheng-Fa Tu(涂成发)[1], Wei Wu(吴伟)[1], Wen-Biao Wang(王文彪)[1], Sheng-Yu Yang(杨晟宇)[1], Sun Zhe(孙哲)[1], Peng Wu(吴鹏)[1], Jin-Bo Yang(杨金波)[2], Chang-Sheng Wang(王常生)[2], Tao Wang(王涛)[1], and Fa-Shen Li(李发伸)[1]

[1] *Institute of Applied Magnetism, Key Laboratory for Magnetism and Magnetic Materials of Ministry of Education, Lanzhou University, Lanzhou* 730000, *China*

[2] *School of Physics, Peking University, Beijing* 100871, *China*

(Received 24 October 2022; revised manuscript received 25 November 2022; accepted manuscript online 2 December 2022)

Intermetallic complexes of rare-earth and 3d transition metals with core-shell structures are commonly employed as microwave absorbing materials due to their high saturation magnetizations and natural resonance in GHz. Hence, we synthesized Y_2Co_{17} alloy via the co-precipitation reduction-diffusion technique, then coated the Y_2Co_{17} magnetic powders with SiO_2 to create Y_2Co_{17}@SiO_2 core-shell structures. The formation of Y_2Co_{17}@SiO_2/polyurethane (PU) at various volume fractions and their magnetic, electromagnetic properties were investigated using x-ray diffraction, scanning electron microscopy, energy dispersive spectroscopy, and vector network analyzer. The microwave absorption characteristics of Y_2Co_{17}@SiO_2/PU were also investigated at various volume fractions. We not only investigate the zero-reflection conditions of the samples with different volume fractions, but also show that every absorber has a strong reflection loss value (RL$\leq$ -65.00 dB) and excellent microwave absorption properties with an average RL of Y_2Co_{17}@SiO_2/PU being below -10 dB at 8 GHz–18 GHz under different thicknesses, showing that the enhancement of microwave absorption performance arises from the balance between permeability and permittivity of absorber.

Keywords: Y_2Co_{17}@SiO_2, Co-precipitation reduction diffusion, microwave absorption, zero-reflection condition, reflection loss

PACS: 42.25.Bs, 75.50.Bb, 76.30.Kg, 78.20.Ci **DOI:** 10.1088/1674-1056/aca7f1

1. Introduction

With the rapid development of wireless communications, such as 5G mobile wireless systems,[1,2] and the widespread use of high-frequency information technology in recent years,[3,4] severe electromagnetic pollution has been created, which has a negative impact on performance of high-frequency electric devices.[5,6] Furthermore, the public is becoming increasingly concerned about the effects of electromagnetic pollution on human health and living environment.[7] Consequently, materials having superior electromagnetic wave absorption in the microwave frequency range are in high demands.[8–10]

In response to the requirement for effective electromagnetic absorbers in various bands, a wide range of materials, including ferrites, dielectric materials, magnetic materials, and carbon, have been used to absorb ectromagnetic radiation, and making significant progress. For example, the work carried out by Wu *et al.*[11] shows the best microwave absorbing property was -16 dB and the relative bandwidth reached 3.9 at 5.5 GHz with the thickness of 3 mm after doping with 1.0 wt% of V_2O_5 in $BaCoZnFe_{16}O_{27}$ composites. Wang *et al.*[12] prepared $Y_2Fe_{16}Si$@MOF and $Y_2Fe_{16}Si$@GO, considerable absorption strength (close to -20 dB), and large absorption bandwidth (4 GHz) within a relatively thin thickness (less than 2.0 mm). Wang *et al.*[13] demonstrated that the optimal RL of the irregular Co particles was -22 dB at 10.5 GHz with the thickness of 1.4 mm and the bandwidth with RL below -10 dB in the whole *X* band at 673 K. Their potential applications, however, were limited due to their low saturation magnetization and resonance frequency.

The planar anisotropy Re_2T_{17} magnetic powders and their diffractors (Re = rare-earth element, T = transition metal element) with outstanding magnetic in GHz have been created in the previous decade, and their microwave absorption characteristics have also been reported.[14–16] The planar anisotropy Re_2T_{17} intermetallics with excellent planar anisotropy properties have been drawing increasing attention due to higher saturation magnetization M_s and resonance frequency f_r compared with ferrite.[17] For the magnetic materials with planar anisotropy, the product of the static susceptibility (μ_0-1) and resonance frequency f_r is given by[18]

$$(\mu_0-1)f_r=\frac{2}{3}\gamma M_s\sqrt{\frac{H_\theta}{H_\phi}}, \tag{1}$$

where μ_0, γ, M_s, H_θ, and H_ϕ are the initial permeability, the gyromagnetic ratio, the saturation magnetization, the out-of-

†Corresponding author. E-mail: qiaoliang@lzu.edu.cn

© 2023 Chinese Physical Society and IOP Publishing Ltd

plane and in-plane anisotropy fields, respectively. H_θ is much larger than H_ϕ resulting in the increasing permeability and resonance frequency.[19] These advantages is conducive to satisfy the impedance matching of the absorbing materials.

The substantial eddy current loss produced by low resistivity restricts the concentration rise of the planar-anisotropy Re_2T_{17} magnetic powders, degrading the materials' magnetic characteristics.[20] One typical technique for overcoming excessive eddy current loss is to cover the powders with non-metallic materials and construct a core-shell structure.[21] These changes are mostly the result of reduced eddy current loss, the coating layer's own dielectric characteristics, and interfacial polarization. In some ways, such a coating layer appears to be a manner of controlling the dielectric characteristics of the materials, although the magnetic properties of the materials are still dictated by the intrinsic properties of the magnetic powders.[22] For example, researchers have realized that Ni@C nanocapsules[23] strengthen the reflection loss in absorber and flower-like FeNi@C nanocomposites[24] enhance microwave absorption of absorber.

Herein, different from all previous methods, we choose to make YCo-hydroxide precursor first, then to reduce these hydroxides to synthesize the planar-anisotropy Y_2Co_{17}, finally, SiO_2 is used to coat Y_2Co_{17} metallic magnetic powders to form $Y_2Co_{17}@SiO_2$ core-shell structures. Y_2Co_{17} is a easy-plane rare earth soft magnetic composite with high saturation magnetization, large magnetocrystalline anisotropy. The microwave absorption properties of $Y_2Co_{17}@SiO_2$/PU are studied, and they show good microwave absorption performance. We can obtain that the zero reflection peak occurs at 9.98 GHz at a reflection loss value of -65.00 dB and the effective attenuation bandwidth (EAB: RL < -10 dB) covers x and k_u bands under different thicknesses.

2. Materials and methods

2.1. Synthesis of Y_2Co_{17} and $Y_2Co_{17}@SiO_2$

The precursor was synthesized by co-precipitation of chloride hexahydrate ($CoCl_2.6H_2O$) yttrium hydroxide $YCl_3.6H_2O$ and sodium hydroxide (NaOH). In a typical synthesis, 24.270 g of $CoCl_2{\cdot}6H_2O$, and 5.655 g of $YCl_3{\cdot}6H_2O$ were dissolved in 1600 ml of deionized water. Then, aqueous NaOH solution was added to the solution dropwise to adjust the pH value to 10 at room temperature. After the reaction ran for 1 h, the mixture was centrifuged at 8000 r/min for 5 min. A green precipitate was obtained and twice rinsed degassed distilled water to wash away sodium chloride (NaCl) and extra NaOH. The green precipitate was further washed with degassed ethanol and dried for 24 h at 80 °C in an oven to obtain mixture of $Y(OH)_3$ and $Co(OH)_2$.

For the synthesis of Y_2Co_{17}, 1.0 g of previously prepared precursor powders were mixed with 1.0 g of calcium (Ca) powders and 0.5 g of anhydrous potassium chloride (KCl). Subsequently, the mixture wrapped in tantalum foil was then put in steel tanks. Afterwards, the boat was placed in tube furnace and heated to 1100 °C at a heating rate of 5 °C/min, which was kept for 2 h under an Ar atmosphere. After cooling the reaction mixture down to room temperature, the product was washed with degassed distilled water many times to dissolve CaO, KCl, and extra Ca. The monodispersed Y_2Co_{17} was collected for further characterization. Followed by ball milling with absolute ethanol to obtain particles of uniform size.

Then, the silicon dioxide coating process was employed to synthesize $Y_2Co_{17}@SiO_2$ particles. In this process, the stirrer was kept rotating to ensure that materials were evenly dispersed in the solution. Firstly, 1 g Y_2Co_{17} (2 μm–5 μm) broken particles were added and dispersed in 150 mL ethanol (99.7 wt%). Secondly, 2 mL 3-aminopropyl triethoxysilane (98 wt%) was added to the solution as a surfactant and the liquid-air interface became milky white after stirring for 10 min. Then, 40 mL deionized water, 20 mL ammonia solution (25 wt%–28 wt%) and 3 mL tetraethyl silicate (98 wt%) were added to the solution successively and the solution will continue to be stirred for 2 h at 180 r/min. Finally, $Y_2Co_{17}@SiO_2$ particles were successfully synthesized and collected after the washing and drying processes.

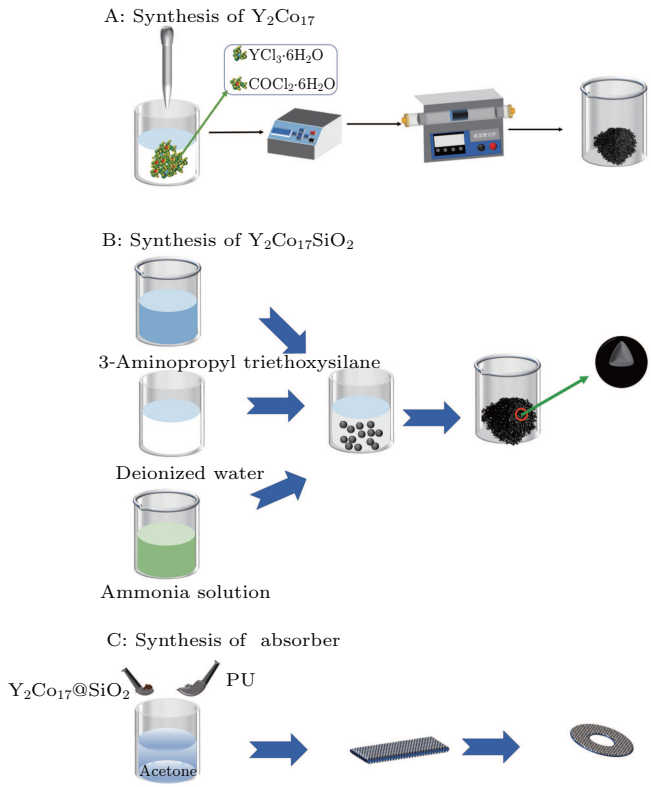


Fig. 1. Process of materials synthesis and absorber preparation.

Synthesis of absorber of magnetic powders and polyurethane (PU): the weighed polyurethane is poured into the appropriate acetone solution and ultrasonicated firstly. Then, different volume fractions (15%, 20%, and 25%) of $Y_2Co_{17}@SiO_2$ magnetic powders were added to the mixtures

as solvent to dissolve the wax with ultrasonic treatment, respectively. These mixture systems keep ultrasonic treatment under stirring until the hexane was evaporated completely. Finally, the solid mixtures were molded to the required ring shape with an inner diameter of 3.04 mm and the outer diameter of 7.00 mm using a mold for measurement to obtain the Y_2Co_{17}@SiO_2/PU absorbers.

The crystal structure of the samples was identified by x-ray diffraction (XRD; Philips, Cu K_α radiation). The static magnetism of the sample was measured by a vibrating sample magnetometer (VSM, Lake Shore 7304) under an applied magnetic field of 20 kOe at room temperature (about 300 K). The size and morphology of Y_2Co_{17} and Y_2Co_{17}@SiO_2 particles after ball milled were observed by scanning electron microscopy imaging (SEM, TESCAN MIRA3). The permittivity and permeability of the samples are measured by a vector network analyzer (VNA, Agilent N5247A) in the 0.1–18 GHz range. The reflection loss of the sample was calculated using the transmission line theory.

3. Results and discussion

3.1. The basic characterization of Y_2Co_{17}@SiO_2

Chemical structure, phase composition properties of the Y_2Co_{17} and Y_2Co_{17}@SiO_2 magnetic powders were analyzed and displayed. The XRD pattern of precursor is shown in Fig. 2(a). Obviously, all the sharp peaks were matched with the standard $Co(OH)_2$ spectrum (PDF#30-0443), and the spectrum without $Y(OH)_3$. The reason for this phenomenon is that $Y(OH)_3$ is amorphous. Figure 2(b) shows the XRD patterns of the Y_2Co_{17} samples. As shown in Fig. 2(b), all the sharp peaks are indexed as Y_2Co_{17} (PDF#18-0434). The sharp peak shape indicates good crystallinity. The diffraction peaks of Y_2Co_{17}@SiO_2 appear in Y_2Co_{17}@SiO_2 samples. The x-ray diffraction peaks of raw Y_2Co_{17} and Y_2Co_{17}@SiO_2 magnetic powders match well with previous work of the rhombohedral Th_2Zn_{17}-type structure. Therefore, the crystalline structure of Y_2Co_{17}@SiO_2 has not been changed during the synthesizing and coating progresses.[25]

Figure 3(a) presents the micromorphology and size of the raw Y_2Co_{17} particles. It exhibits loose and irregular distribution and an overall flaky morphology with average particle size of 2–5 μm. It is known that metallic materials commonly exhibit a significantly skin effect at high frequencies, resisting the transmission of electromagnetic waves into the material. Likewise, Figs. 3(b) and 3(c) exhibit the microscopic morphologies of Y_2Co_{17} (ball-milled) particles and Y_2Co_{17}@SiO_2 particles. In Fig. 3(b), the Y_2Co_{17} particles after ball milling display irregular shapes with smooth surface and the average size of 2–3 μm. The particle size of ball-milled samples is substantially smaller than the skin depth at high frequency, allowing the electromagnetic waves to transmit into the inner part of the absorbers and can be absorbed efficiently. Meanwhile, metal materials generally have a high dielectric, we adopted the form of surface non-magnetic material coating to form a core-shell structure to reduce the dielectric. The size and micromorphology of Y_2Co_{17}@SiO_2 magnetic powders are shown in Fig. 3(c). The size increases to about 3 μm–5 μm because the SiO_2 layer was accumulated continuously by SiO_2 nanoparticles. In addition, Y_2Co_{17}@SiO_2 particles also have irregular shapes and are covered tightly by nano-sized SiO_2 as displayed in Fig. 3(c), which is beneficial for impedance matching.

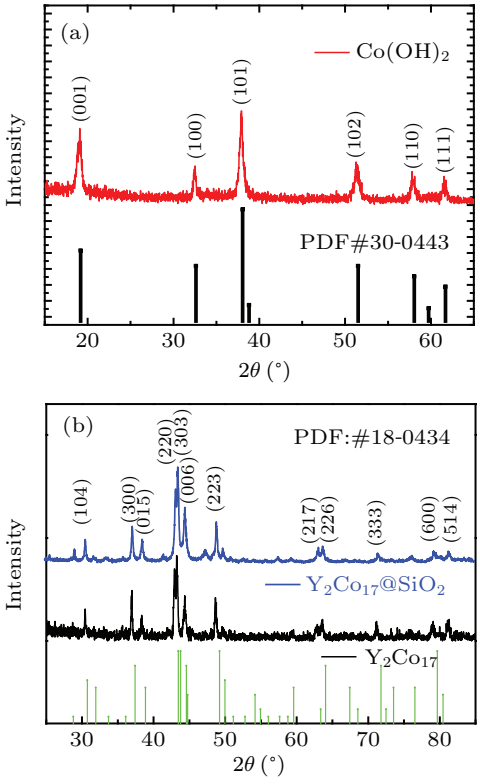


Fig. 2. (a) The XRD pattern of precursor powders. (b) The XRD patterns of the Y_2Co_{17} powders and Y_2Co_{17}@SiO_2 powders.

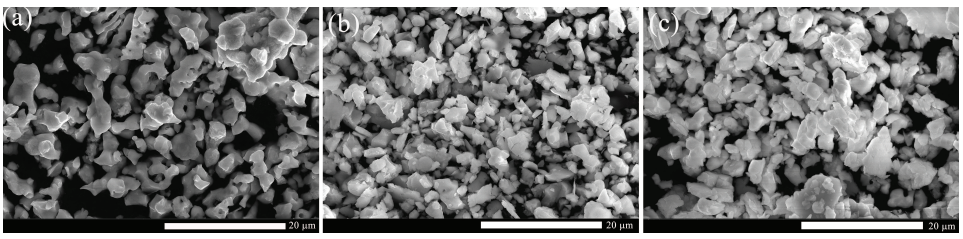


Fig. 3. (a) The SEM images of the raw Y_2Co_{17} particles. (b) The SEM images of the ball-milled Y_2Co_{17} particles. (c) The SEM images of Y_2Co_{17}@SiO_2 particles.

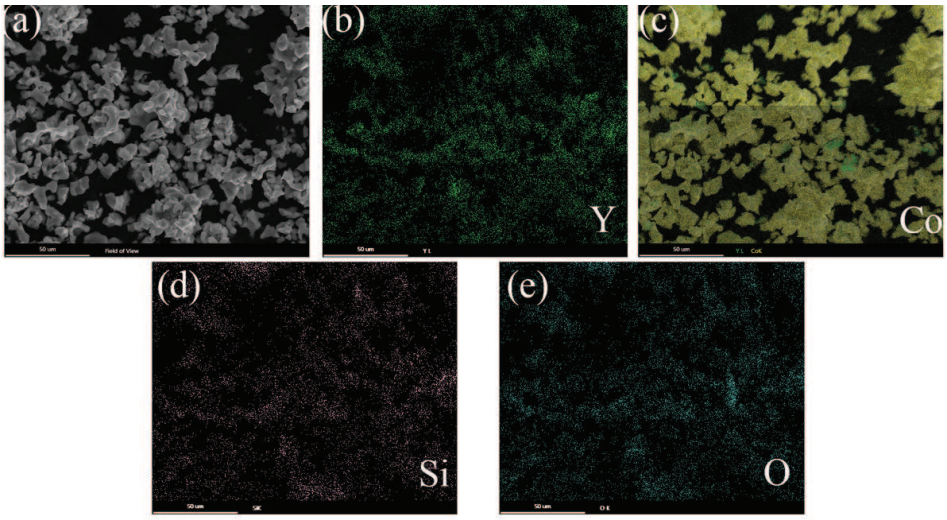


Fig. 4. The elemental mapping images of particles for Y_2Co_{17}@SiO_2 particles.

To further identify the distribution characteristics of the elements after coating, the elemental mapping images of Y_2Co_{17}@SiO_2 particles are shown in Fig. 4. From the elemental mapping images, we can see that the element distribution is highly consistent with the shapes of Y_2Co_{17}@SiO_2 particles, which indicates that SiO_2 coats the surface of particles tightly and evenly, and the flocculent layer improves resistivity and anti-oxidation effectively.

To acquire the static magnetic properties of raw Y_2Co_{17}@SiO_2 powders, the magnetic hysteresis were characterized as shown in Fig. 5(a), the saturation magnetization value of the Y_2Co_{17}@SiO_2 powders decreases from 126.81 emu/g to 113.60 emu/g after silica coating. The saturation magnetization value significantly decreases because of the accession of non-magnetic silica. Furthermore, the in-plane and out-of-plane hysteresis loops of the Y_2Co_{17}@SiO_2/PU composite are shown in Fig. 5(b) as green and red lines, respectively. The red line shows the hysteresis loop measured with the applied magnetic field perpendicular to the sample, which is here considered to be the out-of-plane hysteresis loop, and the black line shows the hysteresis loop measured with the applied magnetic field parallel to the sample, which is considered to be the in-plane hysteresis loop. The in-plane saturation magnetization intensity (M_s) and the out-of-plane residual magnetization intensity ($M_{r,out-plane}$) can be obtained from the two hysteresis loops. Based on the acquisition of the parameters, the degree of plane orientation (DOP) of Y_2Co_{17} composite can be calculated by the following expression:[26]

$$\mathrm{DOP} = \frac{M_s - M_{r,out-plane}}{M_s} \times 100\%. \quad (2)$$

The M_s is 71.70 emu/g and $M_{r,out-plane}$ is 2.96 emu/g from the two hysteresis loops. According to Eq. (2), the DPO is 95.87%, thus the Y_2Co_{17}@SiO_2/PU composites are a kind of easy-plane rare earth soft magnetic composites (Re-SMC).

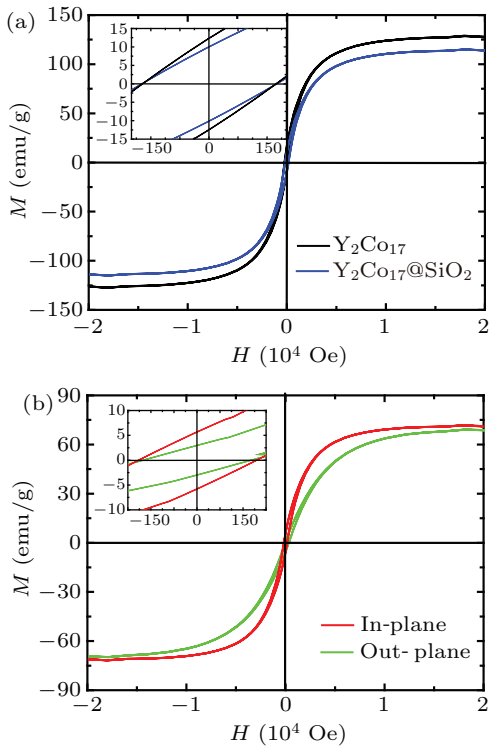


Fig. 5. (a) The hysteresis loop of Y_2Co_{17} powders and Y_2Co_{17}@SiO_2 powders. (b) The hysteresis in-plane and out-of-plane loops of the Y_2Co_{17}@SiO_2/PU composites.

The high-frequency complex permeability (μ_r) and complex permittivity (ε_r) of the Y_2Co_{17}@SiO_2 sample at different volume fractions were measured by the coaxial method at room temperature over 0.1 GHz–18 GHz, as shown in Fig. 6. It can be seen from Fig. 6(a) that the real parts of the permeability of the three samples have a downward trend within 1 GHz–18 GHz, and the value becomes larger with increasing volume fraction of the sample. The imaginary parts of the three samples increase first and then decrease while the frequency goes from 2 GHz to 18 GHz, obvious resonance peaks in Fig. 6(a), we know that the resonance peaks around

1 GHz are natural resonance peaks. Three samples have similar permeability, while their permittivities are different from each other, as shown Fig. 6(b). The reason is that the change of the coating materials may alter the permittivity of the composite materials, while the permeability of the composite materials is mainly determined by the intrinsic properties of the inside magnetic powders.

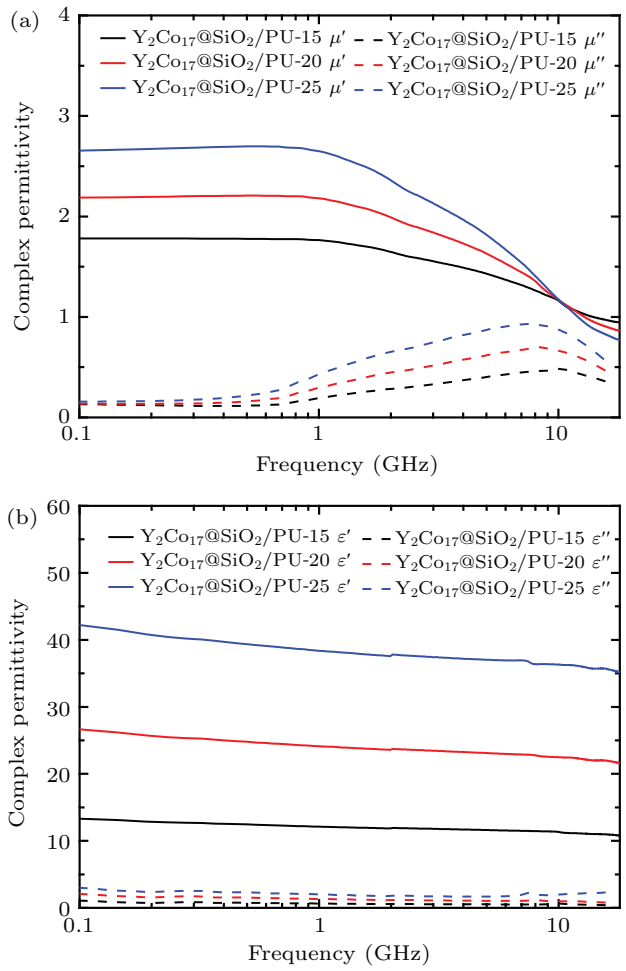


Fig. 6. The electromagnetic parameters of the Y_2Co_{17}@SiO_2/PU composites: (a) the complex permeability of the Y_2Co_{17}@SiO_2/PU composite; (b) the complex permittivity of the Y_2Co_{17}@SiO_2/PU composites.

3.2. Zero reflection parameter related to absorber volume concentration

3.2.1. Zero reflection parameters of Y_2Co_{17}@SiO_2/PU complexes with different volume concentrations

The high-frequency electromagnetic parameters of the samples change slowly with frequency, which provides favorable conditions for achieving good impedance and phase in a wide frequency band. Many of previous works reported that the calculated RL values had been contrasted each other to obtain optimized absorption materials. The reflection loss (RL) is calculated by the transmission line theory.[27,28] The RL and and the quarter-wavelength[29,30] of a single-layer absorber on a metal plate can be calculated by the following formulas:

$$Z_{\text{in}} = Z_0\sqrt{\frac{\mu_{\text{r}}}{\varepsilon_{\text{r}}}}\tanh\left(j\frac{2\pi ft}{c}\sqrt{\mu_{\text{r}}\varepsilon_{\text{r}}}\right), \tag{3}$$

$$\text{RL(dB)} = 20\log_{10}\left|\frac{Z_{\text{in}}-Z_0}{Z_{\text{in}}+Z_0}\right|, \tag{4}$$

$$t = \frac{nc}{4f\sqrt{\mu_{\text{r}}\varepsilon_{\text{r}}}}, \quad n = 1,3,5,\ldots, \tag{5}$$

where Z_{in} is the input impedance of the absorber, Z_0 is the impedance of free space, $z_0 = (\mu_0/\varepsilon_0)^{1/2} = 377\ \Omega$, ε_{r} is the complex permittivity, μ_{r} is the complex permeability, f is the frequency of the electromagnetic wave, t is the thickness of the single-layer absorber, and $c = 3\times10^8$ m/s is the speed of light. From Eqs. (3)–(5), we can see that the reflection loss RL $= -\infty$ and the absorber at $Z_{\text{in}}/Z_0 = 1$, which is the strongest absorption peak on the RL–f curve, exhibit zero reflection of the incident electromagnetic wave ideally. The peak frequency of the strongest reflection loss absorption peak is called the perfectly matched frequency (f_{p}), and the thickness of the absorber is called the perfectly matched thickness (t_{p}), which constitute the perfectly matched condition.

Figures 7–9 show the matched thickness t, the peak point impedance Z_{in}/Z_0 of all reflection peaks, and the reflection loss RL of the perfectly matched absorption peaks with respect to frequency for the Y_2Co_{17}@SiO_2/PU with different volume concentrations. The zero reflection parameters and absorption properties of the compound are listed in Tables 1–3. The zero-reflection frequencies and perfectly matching thicknesses for different volumes of the complexes can be obtained from the quarter-wavelength curve and the Z_{in}/Z_0 values corresponding to each one, and further the zero-reflection loss peaks of the complexes can be calculated. Commonly, the closer to 1 the Z_{in}/Z_0 values, the greater the impedance matching of absorbers. The Z_{in}/Z_0 line of 15% absorber has the intersection with the $Z_{\text{in}}/Z_0 = 1$ line at frequency 10 GHz under the thickness of 1.97 mm; in contrast, the Z_{in}/Z_0 lines of 20% and 25% absorbers have intersection points with the $Z_{\text{in}}/Z_0 = 1$ line at 3.95 and 2.11 GHz under 2.88 and 3.70 mm as shown in Figs. 7 and 8, 9(a) and 9(b), respectively. Then, we obtain the zero reflection loss curves for different volume fraction absorbers, and all of them exhibit good absorption performance. In comparison of the zero-reflection conditions (t_{m}, f_{m}) and the corresponding zero-reflection properties (RL$_{\text{min}}$, Δw) of all the complexes, we observe that the corresponding zero-reflection thickness gradually increases as the volume concentration of the complexes increases, while the zero-reflection frequency point gradually tends to the low frequency range. In addition, the absorption bandwidth ΔW at zero reflection also becomes gradually narrower. In summary, we can present the zero reflection parameters for all materials.

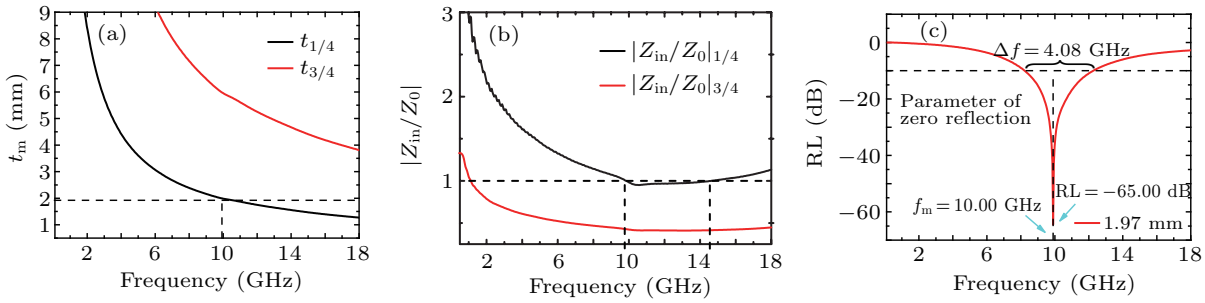


Fig. 7. (a) The $\lambda/4$ and $3\lambda/4$ values calculated from the complex permittivity and permeability. (b) Dependence of input resistance on frequency. (c) Dependence of RL experimental and calculation results on frequency at 1.97 mm for Y_2Co_{17}@SiO_2/PU composite.

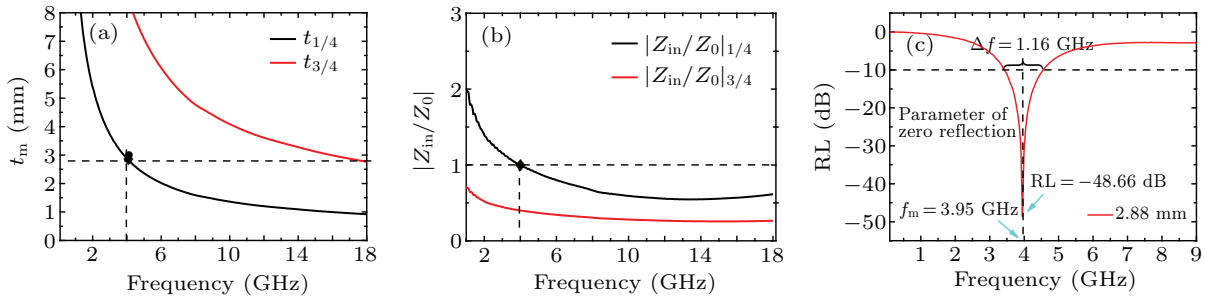


Fig. 8. (a) The $\lambda/4$ and $3\lambda/4$ values calculated from the complex permittivity and permeability. (b) Dependence of input resistance on frequency. (c) Dependence of RL experimental and calculation results on frequency at 2.88 mm for Y_2Co_{17}@SiO_2/PU composite.

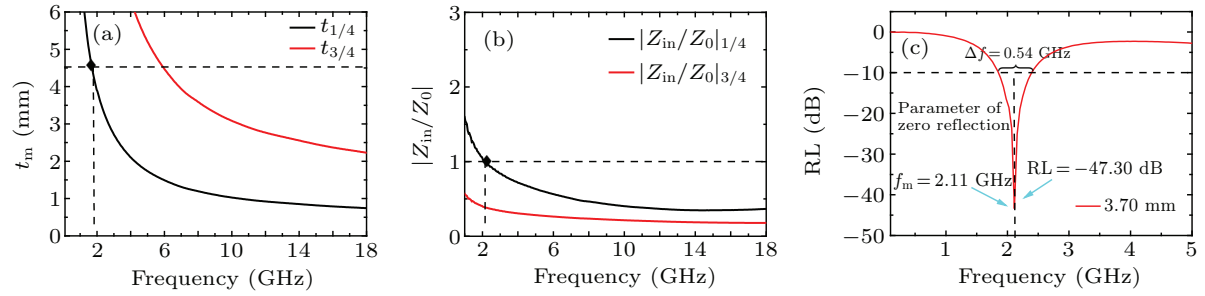


Fig. 9. (a) The $\lambda/4$ and $3\lambda/4$ values calculated from the complex permittivity and permeability. (b) Dependence of input resistance on frequency. (c) Dependence of RL experimental and calculation results on frequency at 3.70 mm for Y_2Co_{17}@SiO_2/PU composite.

Table 1. Zero reflection parameter and absorption performance at perfect match.

Matching parameters	μ	ε	$\sqrt{\varepsilon_r/\mu_r}$	$\sqrt{\mu_r\varepsilon_r}$
	1.17–0.48i	11.4–0.627i	3	3.79
Absorption performance	t_m (mm)	f_m (GHz)	Z_{in}/Z_0	RL (dB)
	1.97	9.98	0.995	−65.00

Table 2. Zero reflection parameter and Absorption performance at perfect match.

Matching parameters	μ	ε	$\sqrt{\varepsilon_r/\mu_r}$	$\sqrt{\mu_r\varepsilon_r}$
	1.17–0.48i	23.3–1.08i	6.52	3.57
Absorption performance	t_m (mm)	f_m (GHz)	Z_{in}/Z_0	RL (dB)
	2.88	3.95	0.987	−48.66

Table 3. Zero reflection parameter and Absorption performance at perfect match.

Matching parameters	μ	ε	$\sqrt{\varepsilon_r/\mu_r}$	$\sqrt{\mu_r\varepsilon_r}$
	2.3–0.667i	37.7–1.79i	3.97	9.51
Absorption performance	t_m (mm)	f_m (GHz)	Z_{in}/Z_0	RL (dB)
	3.70	2.11	0.993	−47.30

3.2.2. The reflection loss at specified frequency

Receiving the zero-reflection parameters and absorber performance is insufficient. Radar devices are generally known to be categorised based on their operating frequency obtained. It is meaningful to apply the microwave absorption performance of the absorber to each waveband. For example, short- and medium-range early warning and tracking radars operate in the S-band at frequencies ranging from 2 GHz to 4 GHz; short- and medium-range tracking and fire control radars operate in the C-band at frequencies ranging from 4 GHz to 8 GHz; and so on.

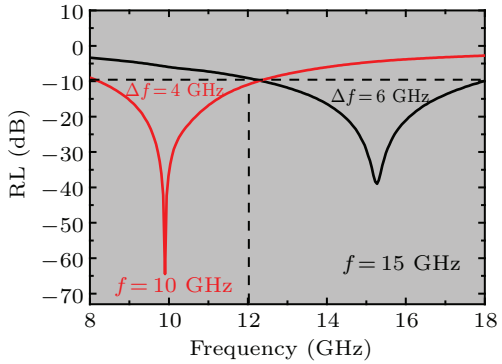


Fig. 10. The dependence of reflection loss on frequency at the specified frequency (10 GHz, 15 GHz).

As an example, we have studied the microwave absorption performance of absorbers with a volume fraction of 15% for each application band. The frequency dependence of the RL values for the composites with various frequencies (10 GHz, 15 GHz) are shown in Fig. 10.

The strength of the absorption decreases gradually with the increase of the frequency, while the frequencies corresponding to RL peaks move to the low frequency direction, which can be explained by the quarter wave theory. We can find that the absorber of Y_2Co_{17}@SiO_2/PU can work perfectly in the X-band (the red lines), and the absorption properties with an average value of reflection loss (RL) being below −10 dB in X band, which can play a good role in frequency closure stealth for the devices working in this band. Also, the absorption properties of Y_2Co_{17}@SiO_2/PU show an average value of reflection loss (RL) being below −10 dB in K_u-band (the black lines). Table 4 displays the absorption performance of each frequency band.

Table 4. The absorption performance of each frequency band.

Wave band	Range (GHz)	RL (dB)	δf (GHz)	d (mm)
X band	8–12	−65.00	4.00	1.97
K_u band	12–18	−38.00	6.00	1.42

3.2.3. The reflection loss at specified thicknesses

Figure 11 depicts the relationship between reflection loss (RL) and microwave frequency f and sample thickness d for Y_2Co_{17}@SiO_2/PU composites. As demonstrated, in Figs. 11(a)–11(c), the microwave absorption characteristics of materials with varying volume concentrations fluctuate dramatically. The Y_2Co_{17}@SiO_2/PU composites exhibit excellent microwave absorption properties with an average of reflection loss (RL) being below −10 dB at 8 GHz–18 GHz. More information is available as seen in Figs. 11(d)–11(f). As displayed in Fig. 11(e), the location of the maximum value of RL moves to the low-frequency region with the increase of thickness, the value of RL first decreases and then increases, and reaches a minimal RL of −65.00 dB at d = 1.97 mm, where the impedance ratio Z_{in}/Z_0 equals 1.

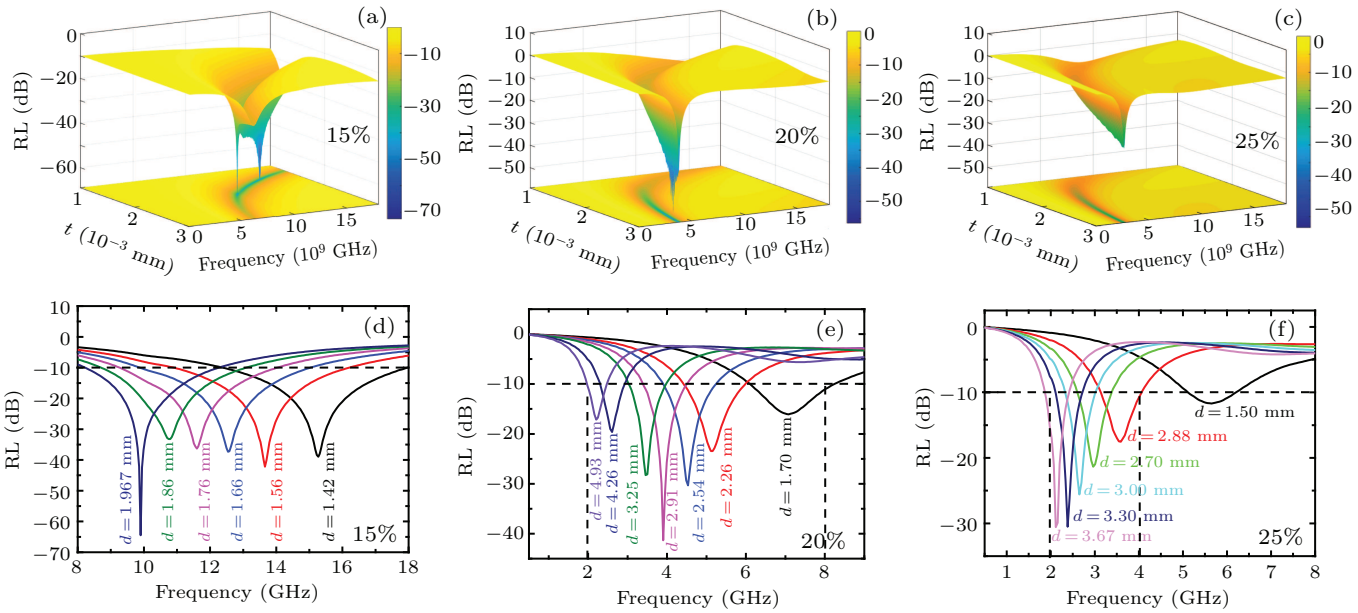


Fig. 11. The wave absorption performance in for Y_2Co_{17}@SiO_2/PU composites.

As we all know, the impedance matching between the composite and air determines the microwave absorption properties. Based on Fig. 6, it is known that three samples have comparable magnetic permeability but vary in permittivity. Only when the volume fraction of the samples is 15%, the difference of permittivity between the two samples becomes smaller, resulting in a better impedance match and optimum better wave absorption performance compared to Y_2Co_{17}/PU composites.[31] Composites of Y_2Co_{17}@SiO_2/PU with a volume fraction of 15% are better candidates for shielding materials in the X-band and K_u-band.

4. Conclusion

In summary, we has synthesized the planar-anisotropy Y_2Co_{17} sample by the co-precipitation reduction diffusion method, followed by ball milling and the formation of a core-shell with SiO_2 cladding. Furthermore, Y_2Co_{17}@SiO_2/PU absorbers are generated. The composition, morphology, static magnetism, high frequency electromagnetic properties, and microwave absorbing properties of Y_2Co_{17}@SiO_2 powders and absorbers are characterized. The zero-reflection parameters (f_p, t_p) for different volume fractions of the absorbing material of the Y_2Co_{17}@SiO_2/PU composites are ob-

tained directly from the measurement data of the electromagnetic parameters. Among various volume concentrations of Y_2Co_{17}@SiO_2/PU composites, the composite with 15 vol% shows excellent microwave absorbing properties in X and K_u bands: an average value of reflection loss (RL) less than −10 dB at different thicknesses.

Acknowledgements

Project supported by the National Key Research and Development Program of China (Grant No. 2021YFB3501302), the National Natural Science Foundation of China (Grant No. 51731001), and the Fund from the State Key Laboratory of Baiyunobo Rare Earth Resource Researches and Comprehensive Utilization's Key Research and Development Projects.

References

[1] Won H Y, Hong Y K, Choi M, Garcia H, Shin H, Yoon Y S, Lee K, Xin H and Yeo C D 2022 *J. Magn. Magn. Mater.* **560** 169523
[2] Zhang X M, Liu Y, Liu Z Y, Wang Y Q, Wang Y and Kong L B 2022 *J. Magn. Magn. Mater.* **560** 169647
[3] Wang X Y, Y. Liang, Wei S C, Wang Y J, Yuan Y, Li L W, Wang B and Xie H J 2022 *J. Magn. Magn. Mater.* **560** 169450
[4] Wang Y Q, Wang H G, Ye J H, Shi L Y and Feng X 2020 *J. Magn. Magn. Mater.* **383** 123096
[5] Zhang H Z, Jia Z R, Feng A L, Zhou Z H, Zhang C H, Wang K K, Liu N and Wu G L 2020 *Compos. Commun.* **19** 42
[6] Gu X S, Tan G G, Chen S W, Man Q K, Chang C T, Wang X M, Li R W, Che S L and Jiang L Q 2017 *J. Magn. Magn. Mater.* **424** 39
[7] He G H, Duan Y P and Pang H F 2020 *Nano-Micro Lett.* **12** 57
[8] Song Y, Yin F X, Zhang C W, Guo W B, Han L Y and Yuan Y 2017 *Nano-Micro Lett.* **13** 1
[9] Gao S T, Zhang Y C, Xing H L and Li H X 2020 *Chem. Eng. J.* **389** 124149
[10] Guan B W, Ding D H, Wang L F, Wu J Y and Xiong R 2017 *Mater. Res. Express* **4** 056103
[11] Wu Y P, Ong C K, Li Z W, Chen L F Lin G Q and Wang S J 2005 *J. Appl. Phys.* **97** 063909
[12] Wang Y K, Liu Z, Zhang P Y, Cai K T, Yang W Y, Han J Z, Liu S Q, Wang C S, Zou R Q and Yang J B 2021 *AIP Adv.* **11** 015237
[13] Wang G W, Li X L, Wang P, Zhang J M, Wang D, Qiao L, Wang T and Li F S 2018 *J. Magn. Magn. Mater.* **456** 92
[14] Tereshina I S, Veselova S V, Verbetsky V N, Paukov M A, Gorbunov D L and Tereshina-Chitrova E A 2022 *J. Alloys Compd.* **897** 163228
[15] Jaballah H, Bouzidi W, Fersi R, Mliki N and Bessais L 2022 *J. Phys. Chem. Solids* **161** 110438
[16] Yang J B, Yang W Y, Li F S and Yang Y C 2020 *J. Magn. Magn. Mater.* **497** 165961
[17] Han R, Yi H B, Zuo W L, Wang T, Qiao L and Li F S 2012 *J. Magn. Magn. Mater.* **324** 2488
[18] Qiao G Y, Hu Q W, Zhang P Y, Yang W Y, Liu Z, Liu S Q, Wang C S and Yang J B 2020 *J. Alloys Compd.* **825** 154179
[19] Gu X S, Tan G G, Chen S W, Man Q K, Chang C T, Wang X M, Li R W, Che S L and Jiang L Q 2017 *J. Magn. Magn. Mater.* **424** 39
[20] Zhang X F, Dong X L, Huang H, Liu Y Y, Wang W N, Zhu X G, Lv B, Lei J P and Lee C G 2006 *Appl. Phys. Lett.* **89** 053115
[21] Chen Y J, Gao P, Zhu C L, Wang R X, Wang L J, Cao M S and Fang X Y 2009 *J. Appl. Phys.* **106** 054303
[22] Jazirehpour M and Seyyed Ebrahimi S A 2015 *J. Alloys Compd.* **639** 280
[23] Li Z X, Ding X L, Li F, Liu X G, Zhang S H and Long H M 2017*J. Phys. D: Appl. Phys.* **50** 445305
[24] Chao F, Liu X G, Sun Y P, Jin C J and Lv Y H 2014 *RSC Adv.* **4** 22710
[25] Zhuang X H, Tan G G, Li F, Ning M Q, Qi C Y, Ge X J, Yang Z and Man Q 2021 *J. Alloys Compd.* **50** 445305
[26] Wu P, Zhang Y D, Hao H B, Qiao L, Liu X, Wang T and Li F S 2022 *J. Magn. Magn. Mater.* **883** 160835
[27] Wang Y K, Lin Z C, Liu Z, Qiao G Y, Zhang P Y, Li K W, Yang W Y, Han J Z, Liu S Q, Wang C S, Qiao L and Yang J B 2022 *IEEE Trans. Magn.* **58** 1
[28] He D L, Dou Z Y, Zhang J M, Wang P, Wang G W, Duan B F, Qiao L and Wang T 2020 *J. Magn. Magn. Mater.* **322** 167191
[29] Kong I, Ahmad H A, Abdullah M H, Hui D, Yusoff A N and Puryanti D 2010 *J. Magn. Magn. Mater.* **513** 3401
[30] Inui T, Konishi K and Oda K 1999 *IEEE Trans. Magn.* **35** 3148
[31] Tu C F, Zheng Z Y, Qiao L, Hao H B, Ma Y G, Sun Z, Wang H, Wang T and Li F S 2020 *Acta Phys. Sin.* **71** 184201 (in Chinese)